



Supplementary Materials for
The Cellular and Molecular Origin of Tumor-associated Macrophages

Ruth A. Franklin, Will Liao, Abira Sarkar, Myoungjoo V. Kim,
Michael R. Bivona, Kang Liu, Eric G. Pamer, & Ming O. Li

Correspondence to: lim@mskcc.org

This PDF file includes:

Materials and Methods
Figures S1 to S18

Materials and Methods

Mice

MMTV-PyMT mice (Jackson Laboratory) were backcrossed to the C57BL/6 background for 10 generations. *Flt3l*^{-/-} and CD45.1⁺ congenic mice were purchased from Taconic Farms. *Ii4*^{-/-}, *Rag1*^{-/-}, and R26-stop-YFP reporter mice were purchased from Jackson Laboratory. *Rbpj*^{fl/fl} mice were provided by Tasuku Honjo and crossed to CD11c^{cre} mice provided by Boris Reizis. *Ccr2*^{-/-}, CCR2^{DTR}, and CCR2^{GFP} reporter mice were provided by Eric Pamer. Littermate controls were used in all experiments when possible. *Rbpj*^{fl/fl} mice were used as wild type controls in CD11c^{cre}*Rbpj*^{fl/fl} PyMT experiments when possible. All mice were maintained in a specific pathogen-free facility and animal experimentation was conducted in accordance with institutional guidelines.

Parabiosis

Parabiotic mice were generated as reported (31) using female 6-8 week old age- and weight-matched CD45.1⁺ or CD45.2⁺ PyMT mice and maintained for approximately 12 weeks post-surgery. Briefly, matching skin incisions were made from the elbow to the knee of each mouse. Forelimb and hindlimb connections were made with sutures and skin incisions were closed using woundclips. Tumors were isolated for analysis from only the unconnected side of each parabiotic partner.

Monocyte depletion and transfer

For depletion of CCR2⁺ monocytes, 16-week-old CCR2^{DTR} PyMT mice were injected i.p. with 5 µg/kg diphtheria toxin (DT, Sigma) every 3 days for 7 total treatments. For monocyte transfer experiments, bone marrow from CCR2^{GFP} mice was collected and depleted of neutrophils, T cells, B cells, and DCs using rat anti-mouse antibodies for Ly6G (Eric Pamer), CD4, CD8, and MHCII (Bio X Cell) in combination with goat anti-rat BioMag beads (Qiagen). The depleted bone marrow was then sorted based on GFP-positivity (for transfer of “CCR2⁺ BM cells”), or based on GFP-positivity and c-Kit and Flt3 negativity (for transfer of “CCR2⁺ BM monocytes”). The sorted cells were injected i.v. into congenically-marked CCR2^{DTR} recipient mice that received DT 24 hours prior to transfer.

Tumor measurement

Tumors were measured weekly using a caliper, beginning when a single tumor diameter reached approximately 5 mm. Tumor volume was calculated using the equation (L x W²) x 0.52 where “L”=length and “W”=width. Individual tumor volumes were added together to calculate total tumor burden.

Immune cell isolation

Tumor tissues from sacrificed mice were prepared by mechanical disruption followed by 1 ¼ hr treatment with 280U/ml Collagenase Type 3 (Worthington Biochemical) and 4 µg/ml DNase I (Sigma) at 37°C with periodic vortexing. Digested tissues were mashed through 70 µm filters, layered in a 44% and 66% Percoll gradient (Sigma), and centrifuged at 3000 rpm for 30 min without brake. Cells at the interface were collected and analyzed by flow cytometry.

Flow cytometry

Fluorochrome-conjugated or biotinylated antibodies against CD45.1 (clone 104), CD45.2 (A20), MHCII (M5/114.15.2), CD11c (N418), TCR-β (H57-597), CD4 (RM4-5), CD8

(17A2), PD-1 (RMP1-30), CD115 (AFS98), F4/80 (BM8), c-Kit (2B8), BTLA (8F4), and Flt3 (A2F10) were purchased from eBioscience. Antibodies against CD45 (clone 30-F11), Ly6C (AL-21), Ly6G (1A8), B220 (RA3-6B2), CD26 (H194-112), CD64 (X54-5/7.1), Ki67 (B56), and Vcam1/CD106 (429) were purchased from BD Biosciences. Anti-CD11b (clone M1/70) and anti-GzmB (GB11) were purchased from Invitrogen. Anti-MerTK was purchased from R&D Systems (#BAF591). Anti-Mrc1/CD206 was purchased from BioLegend (C068C2). All antibodies were tested with their respective isotype controls. Splenocytes were digested with 4000U/ml Collagenase Type 3 for 35 min, incubated with 10mM EDTA for 5 min, and depleted of erythrocytes by hypotonic lysis. Cells were incubated with specific antibodies for 30 min on ice in the presence of 2.4G2 mAb to block FcγR binding. Ki67, Mrc1, and GzmB staining were carried out using the intracellular cytokine staining kit from eBioscience. Incorporation of EdU was measured using the Click-iT EdU flow cytometry assay kit according to the manufacturer's instructions (Invitrogen). Mice were injected i.p. with 50μg/g EdU and sacrificed 20 hours later. All samples were acquired with a LSRII flow cytometer (Becton Dickinson) and analyzed with FlowJo software (Tree Star).

Cytospin

FACS sorted cells (populations I-III) were loaded on slides using the Cytospin 4 (Thermo Scientific) and dried slides were stained with the Diff-Quik Wright-Giemsa Stain Set (Dade Behring). Images were captured at an original magnification of 40x using a Zeiss Axioplan 2 widefield microscope.

Microarray and computational analysis

CD11b⁺ splenic DCs, TAMs, and MHCII⁺ cells (from CD11c^{cre}Rbpj^{fl/fl} mice) were isolated from 20-week-old PyMT mice by FACS and RNA was prepared with the miRNeasy Mini Kit according to the manufacturer's instructions (Qiagen). MTMs and TAMs from 16-week-old PyMT mice were sorted directly into Trizol (Sigma). RNA isolation, amplification, labelling, and hybridization to M430 2.0 chips (Affymetrix) were carried out at the Genomics Core Facility of Memorial Sloan Kettering Cancer Center. Probe expression levels were calculated by quantile normalization and summarized using median polish as implemented in the robust multi-array (RMA) procedure (32) available via the *affy* BioConductor package for the R statistical software project. Differentially expressed genes were determined using the *limma* BioConductor package with a *p*-value threshold of 0.05. Expression levels were preprocessed prior to principal component analysis (PCA), which entailed mean-centering of gene-level log-transformed expression values. Principal component rotations were determined from a training set comprised of published data for DC CD103⁺ (lung), DC CD103⁺ (SI), DC CD4⁺, DC CD8⁺, MF CD11b⁺ (lung), MF CD11b⁺ (SI), Microglia, and MF RP from the Immunological Genome Project (GSE15907) and tested using Leave-one-out cross-validation. Class predictions were made on the test set of DC CD11b⁺ and TAM (mammary) expression data. A secondary classification procedure, a support vector machine (SVM) classifier (33), was used on the normalized expression values to corroborate the PCA predictions. The SVM was trained on the same data set as in the PCA analysis to categorize dendritic cells and macrophages, again employing a Leave-one-out cross validation scheme, and the resulting model was used to predict the probabilities of the test set belonging to either of the classes.

Quantitative real-time PCR

Total RNA was isolated from sorted CD11b⁺ spDCs, TAMs, or MTMs using the RNeasy Mini Kit, including on-column DNase digestion with the RNase-Free DNase Set

according to the manufacturer's instructions (Qiagen). cDNA was synthesized using the QuantiTect Reverse Transcription Kit (Qiagen) and qPCR was carried out with the QuantiTect SYBR Green PCR Kit (Qiagen). The mRNA levels of *Zbtb46*, *Mafb*, *Fizz1*, *Mrc1*, *Ym1*, and *Actb* were determined by qPCR using the following primers: *Zbtb46* 5'-agagagcacatgaagcgaca-3' and 5'-ctggctgcagacatgaacac-3'; *Mafb* 5'-ggggcceaattgacatacac-3' and 5'-cttaggacgcaaagcctgtc-3'; *Fizz1* 5'-cccttctcatctgcatctcc-3' and 5'-aggaggcccatctgttcata-3'; *Mrc1* 5'-atgccaagtgggaaaatctg-3' and 5'-tgtagcagtggcctgcatag-3'; *Ym1* 5'-ccagcatatgggcatacctt-3' and 5'-cagacctcagtgctccttc-3'; *Actb* 5'-tgttaccaactgggacgaca-3' and 5'-ggggtgtgaaggtctcaaa-3'. Relative expression was determined using the delta Ct method.

Statistical analysis

Student's *t*-test was used to calculate statistical significance for difference in a particular measurement between groups. A *P* value of <0.05 was considered statistically significant.

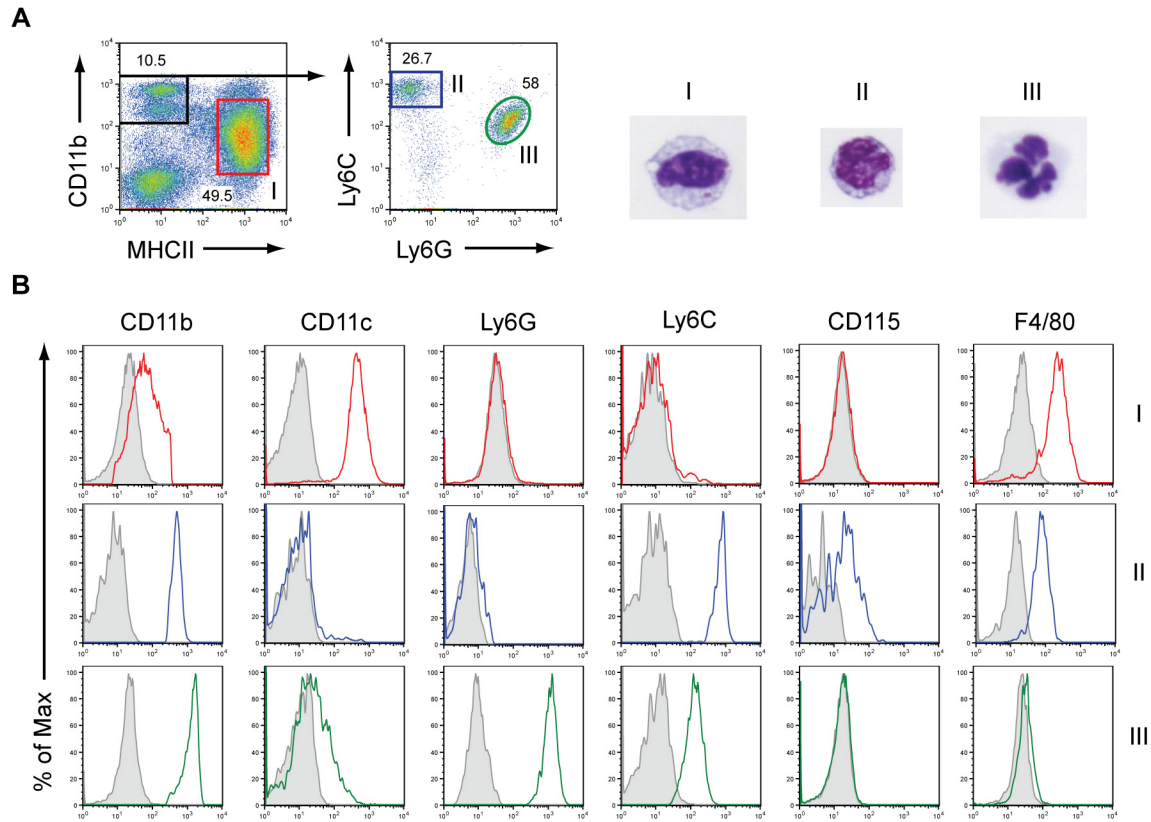


Figure S1. The Myeloid Population Infiltrating MMTV-PyMT Mammary Tumors is Heterogeneous

(A) Gating strategy of myeloid cells from tumors of a 20-week-old PyMT mouse. Cells are gated on $CD45^+$ (left panel) and $CD11b^+$ $MHCII^-$ leukocytes (right panel). Representative images of cells sorted from Populations I-III, after cytopsin and Giemsa staining at an original magnification of 40x. **(B)** Flow cytometric analysis of Populations I-III as gated in **(A)**. Data are representative of at least 3 independent experiments.

		DC	MF	C-V
Training	DC CD103 ⁺ (lung)	0.981314	0.018686	+
	DC CD103 ⁺ (SI)	0.981369	0.018631	+
	DC CD4 ⁺	0.981327	0.018673	+
	DC CD8 ⁺	0.981345	0.018655	+
	MF CD11b ⁺ (lung)	0.013799	0.986201	+
	MF CD11b ⁺ (SI)	0.013795	0.986205	+
	Microglia	0.013815	0.986185	+
	MF RP	0.013786	0.986214	+
Test	DC CD11b ⁺ (sp)	0.910483	0.089517	
	TAM (mammary)	0.068456	0.931544	

Figure S2. Cells of “Population I” are Macrophages

A support vector machine (SVM) classifier was used on the normalized expression values obtained from microarray analysis. The SVM was trained on data sets from the Immunological Genome Project (GSE15907) employing a Leave-one-out cross validation scheme. The probability of each set belonging to the dendritic cell (DC) or macrophage (MF) group is listed. C-V indicates cross validation.

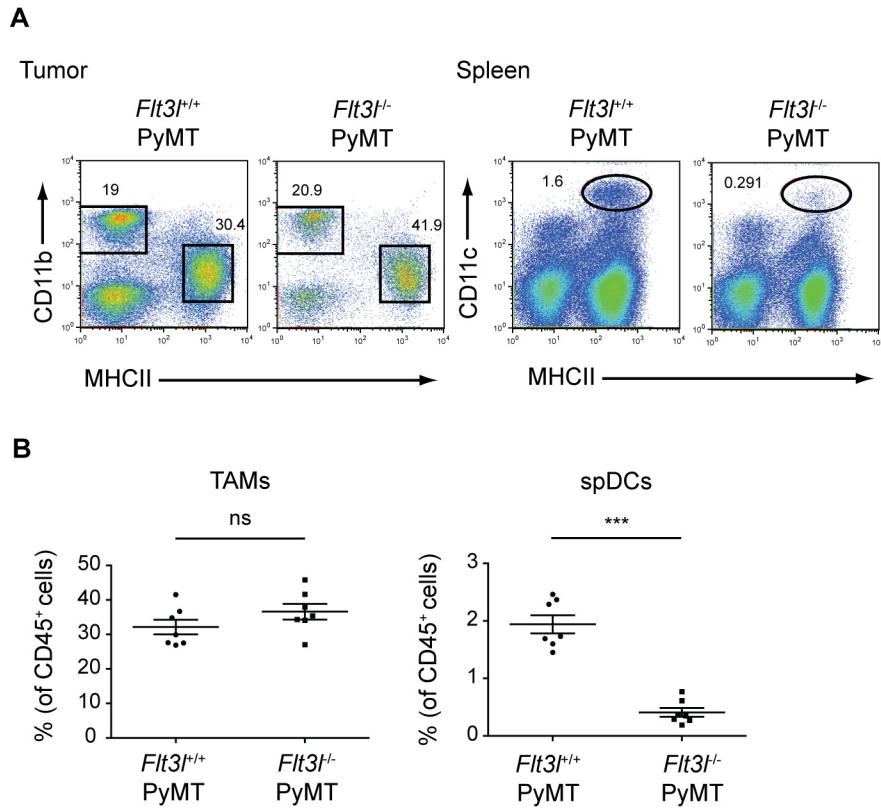


Figure S3. TAMs Originate Independently of Flt3L

(A) Flow cytometric analysis of TAMs or MHCII⁺CD11c⁺ splenic DCs (spDCs) in *Flt3^{+/+}* or *Flt3^{-/-}* PyMT mice. (B) Quantification of TAMs and spDCs (gated on CD45⁺ cells) as in (A) (n=7). Results represent pooled data from at least 3 independent experiments and are shown as mean ± SEM. Student's *t* test was performed and statistical significance is indicated by ***p< 0.001; ns=not statistically significant.

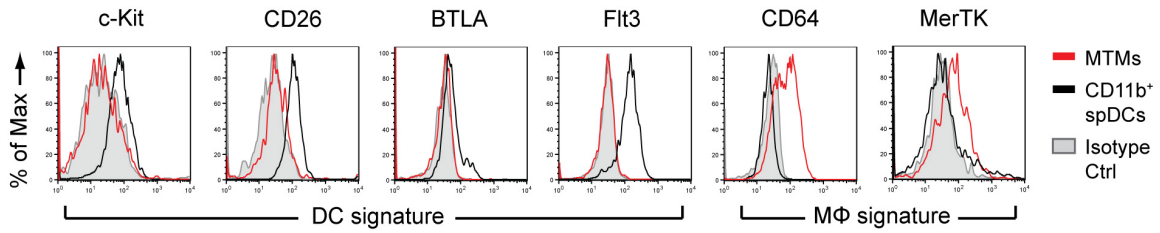


Figure S4. MTMs Phenotypically Resemble Macrophages

Cell surface expression of DC and macrophage signature genes expressed on MTMs and CD11b⁺ splenic DCs as measured by flow cytometry. Data are representative of 2 independent experiments.

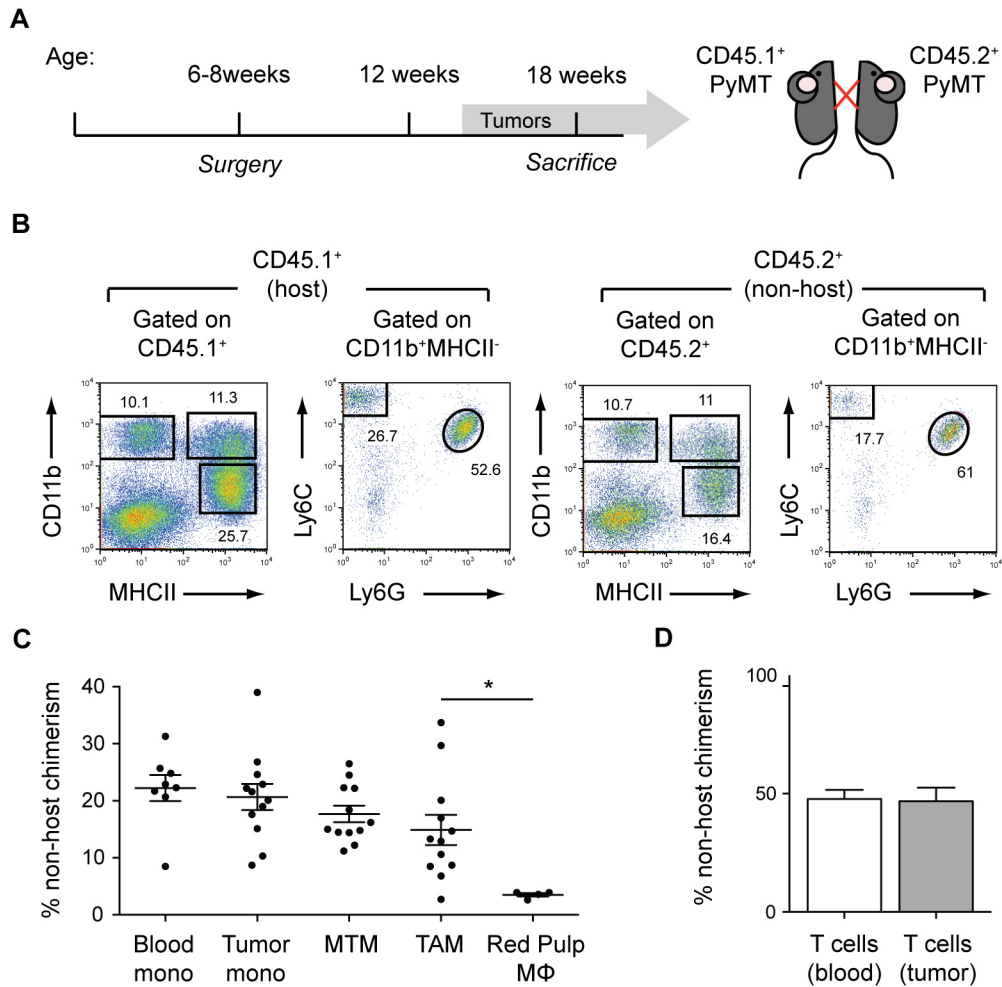


Figure S5. Blood-Borne Precursors Contribute to the TAM and MTM Populations

(A) Graphical representation of parabiosis experiments. **(B)** Representative flow cytometric plots showing myeloid cell populations present in a CD45.1⁺ parabiont (host) ~3 months post-surgery. **(C)** Percentage of myeloid cell non-host chimerism in CD45.1⁺ and CD45.2⁺ parabionts. Blood and tumor monocytes (mono) are gated on CD11b⁺MHCII⁻Ly6C⁺Ly6G⁻ cells (n=8-12). **(D)** Percentage of T cell non-host chimerism in the blood and tumors of CD45.1⁺ and CD45.2⁺ parabionts (n=8). Data are pooled from individual parabiotic partners and are shown as mean ±SEM. Student's *t* test was performed and statistical significance is indicated by **p* < 0.05.

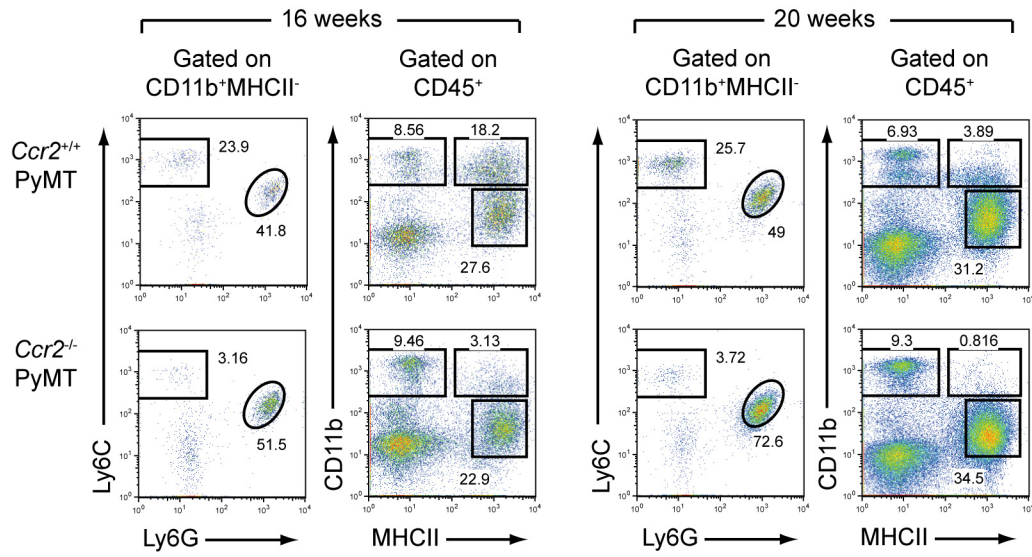


Figure S6. Monocytes and MTMs are Diminished in CCR2-deficient PyMT Mice

Flow cytometric analysis of tumor-associated myeloid cells from 16- and 20- week-old *Ccr2*^{+/+} PyMT and *Ccr2*^{-/-} PyMT mice. Data are representative of 5 independent experiments.

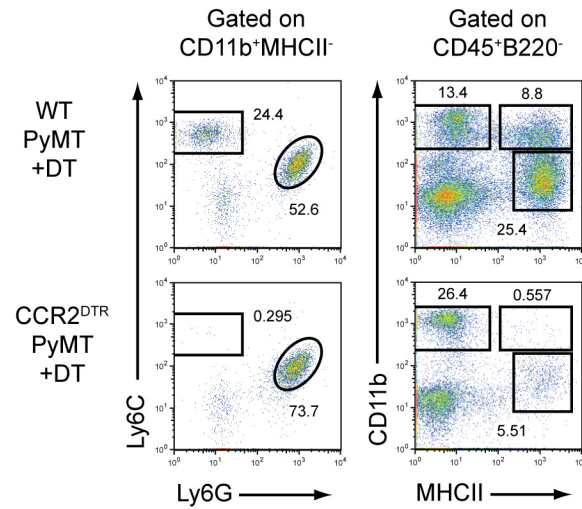
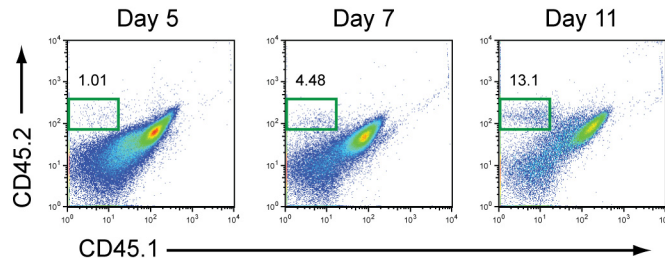


Figure S7. Potent Monocyte Depletion Results in a Reduced TAM Population

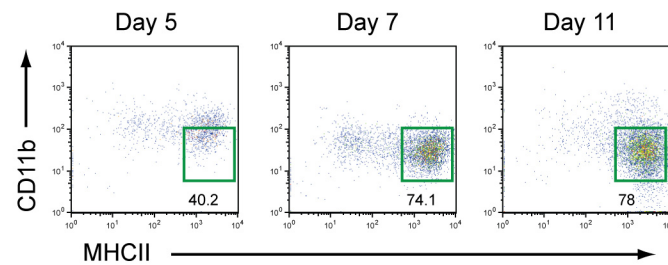
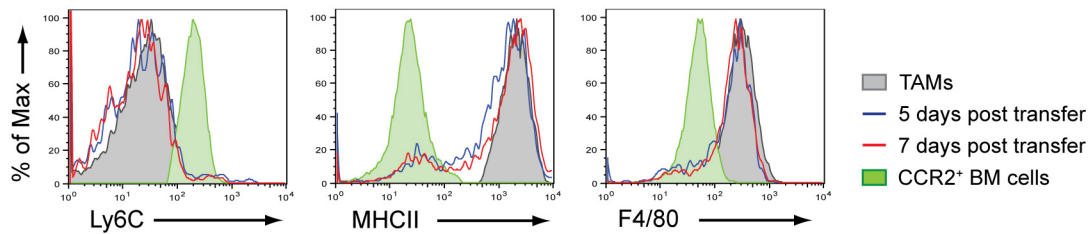
Flow cytometric analysis of tumor-associated myeloid cells from WT PyMT and CCR2^{DTR} PyMT mice after DT treatment (mice were treated i.p. every 3 days, 7 treatments total). Data are representative of 4 independent experiments.

ADonor: CCR2^{GFP} 45.2/45.2 (CCR2⁺ BM cells)Recipient: CCR2^{DTR} PyMT 45.1/45.2

Gated on live cells



Gated on donor cells

**B**Gated on total transferred CCR2⁺ BM cells**Figure S8. Transferred CCR2⁺ Bone Marrow Cells Differentiate into TAMs *in vivo***

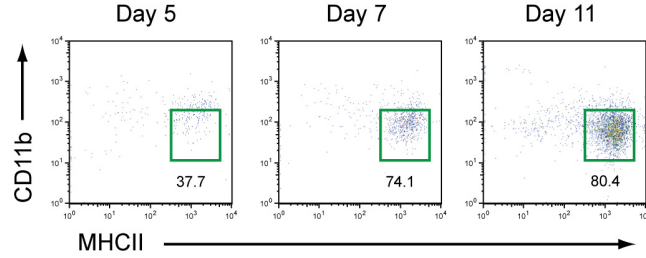
(A) Flow cytometry of congenically marked CCR2⁺ bone marrow (BM) cells 5, 7, and 11 days post transfer into CCR2^{DTR} PyMT mice gated on total live cells (top panel) or total transferred cells (bottom panel). **(B)** Surface expression of Ly6C, MHCII, and F4/80 on transferred BM cells from CCR2^{GFP} mice 5 and 7 days post transfer. Data are representative of 3 independent experiments.

A

Donor: CCR2^{GFP} 45.2/45.2 (CCR2⁺ Flt3⁻ c-Kit⁻ BM monocytes)

Recipient: CCR2^{DTR} PyMT 45.1/45.2

Gated on donor cells



B

Gated on total transferred CCR2⁺ Flt3⁻ c-Kit⁻ BM monocytes

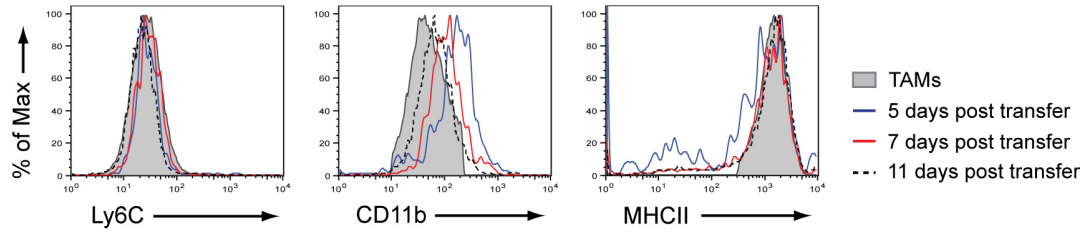


Figure S9. CCR2⁺ Monocytes Give Rise to TAMs *in vivo*

(A) Flow cytometry of congenically marked CCR2⁺Flt3⁻c-Kit⁻ bone marrow (BM) monocytes 5, 7, and 11 days post transfer into CCR2^{DTR} PyMT mice gated on total transferred cells. (B) Surface expression of Ly6C, CD11b, and MHCII on transferred BM monocytes from CCR2^{GFP} mice 5, 7, and 11 days post transfer. Data are representative of 2 mice per time point.

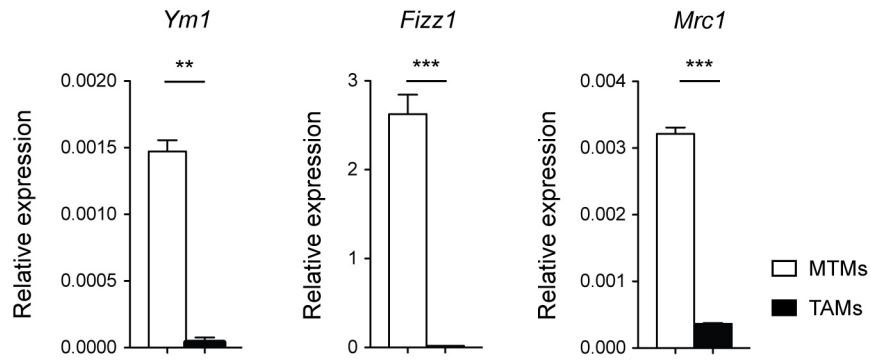


Figure S10. TAMs do not Express AAM Markers

Expression of *Ym1*, *Fizz1*, and *Mrc1* mRNA in sorted MTMs and TAMs from 16-week-old PyMT mice relative to *Actb* as determined by qPCR (n=3). Data are shown as mean \pm SEM. Student's *t* test was performed and statistical significance is indicated by ** $p < 0.01$, *** $p < 0.001$.

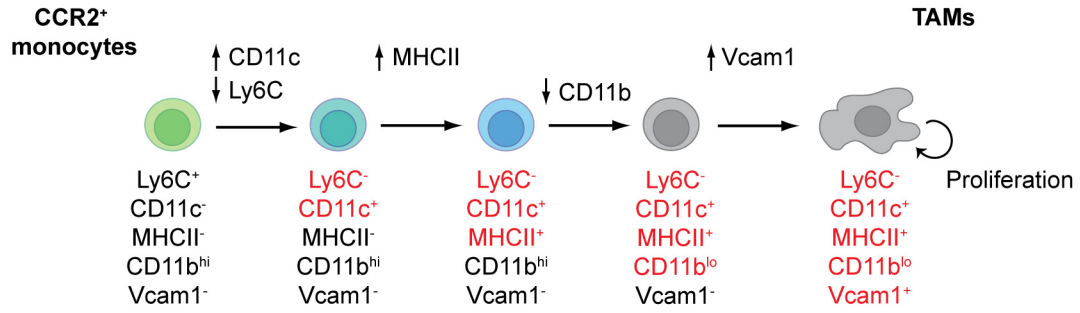


Figure S11. Monocytes Undergo Sequential Phenotypic Changes During Differentiation into TAMs

A schematic representation of intermediate stages of TAM differentiation from monocytes based on data from transfer experiments. Ly6C downregulation and CD11c upregulation are early events, followed by MHCII upregulation, CD11b downregulation, and lastly, Vcam1 upregulation.

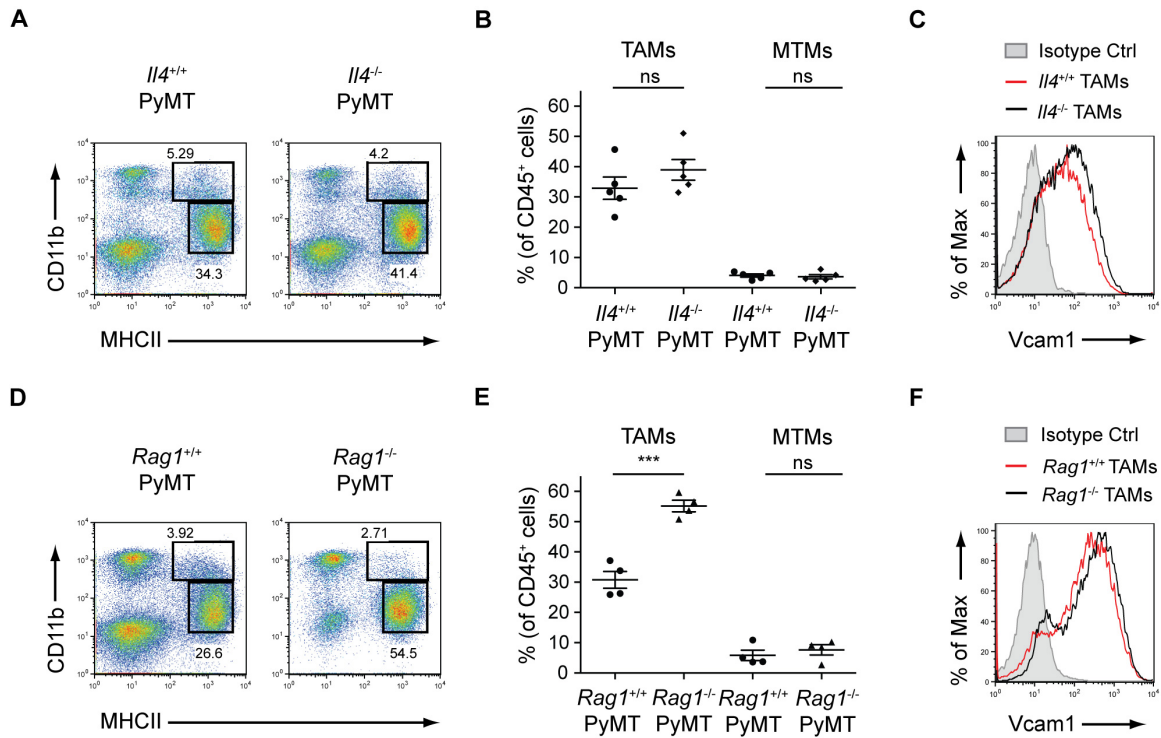


Figure S12. TAM Differentiation does not Require IL-4 or the Adaptive Immune System

(A) Representative flow cytometric data of myeloid populations in $Il4^{+/+}$ PyMT and $Il4^{-/-}$ PyMT mice. (B) Quantification of multiple mice as in (A) ($n=5$). (C) Vcam1 expression on TAMs from $Il4^{+/+}$ PyMT and $Il4^{-/-}$ PyMT mice. (D) Representative flow cytometric data of myeloid populations in $Rag1^{+/+}$ PyMT and $Rag1^{-/-}$ PyMT mice. An increase in the proportion of TAMs in $Rag1^{-/-}$ mice is due to the absence of T and B cells. (E) Quantification of multiple mice as in (D) ($n=4$). (F) Vcam1 expression on TAMs from $Rag1^{+/+}$ PyMT and $Rag1^{-/-}$ PyMT mice. Data are pooled from 4 independent experiments (B, E). All comparisons were made using student's t test and data are shown as mean \pm SEM. Statistical significance is indicated by *** $p < 0.001$; ns=not statistically significant.

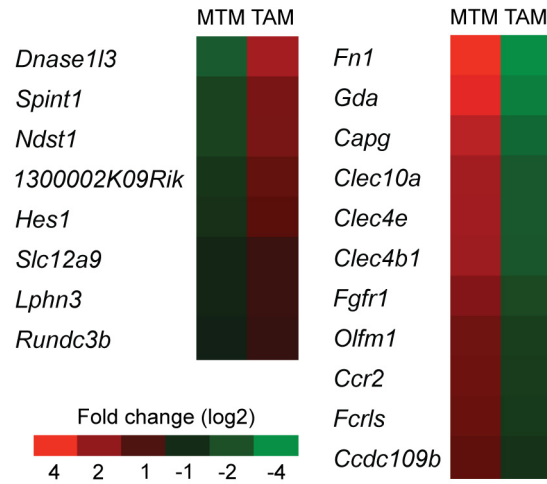


Figure S13. TAMs Exhibit a Notch-dependent Transcriptional Program

Differential expression of Notch-dependent genes between MTMs and TAMs from 16-week-old PyMT mice. Data are pooled from 3 replicate microarray experiments (2 MTM samples and 3 TAM samples). Differentially expressed genes were determined with a *p*-value threshold of 0.05. Fold change is depicted using a log scale.

CD11c^{cre}R26-stop-YFP reporter PyMT

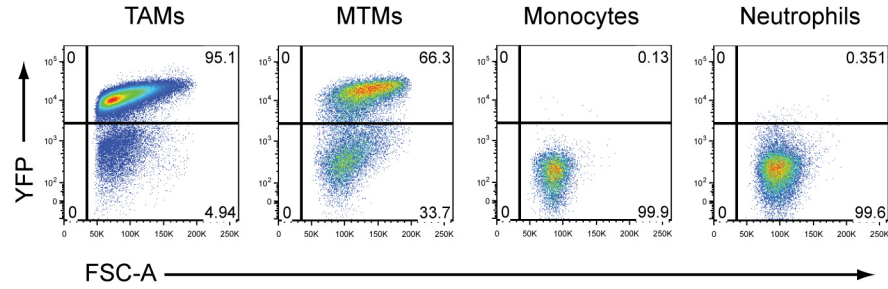


Figure S14. *CD11c^{cre}* Efficiently Deletes Floxed DNA sequences in TAMs

Flow cytometric data showing Cre recombinase activity in TAMs, MTMs, monocytes, and neutrophils from *CD11c^{cre}R26-stop-YFP* reporter mice crossed to the PyMT background. Cell populations were gated as follows: $CD45^+MHCII^{hi}CD11b^o$ (TAMs), $CD45^+MHCII^{hi}CD11b^{hi}$ (MTMs), $CD45^+CD11b^+MHCII^-Ly6C^+Ly6G^-$ (monocytes), and $CD45^+CD11b^+MHCII^-Ly6C^+Ly6G^+$ (neutrophils). Data are representative of 3 independent experiments.

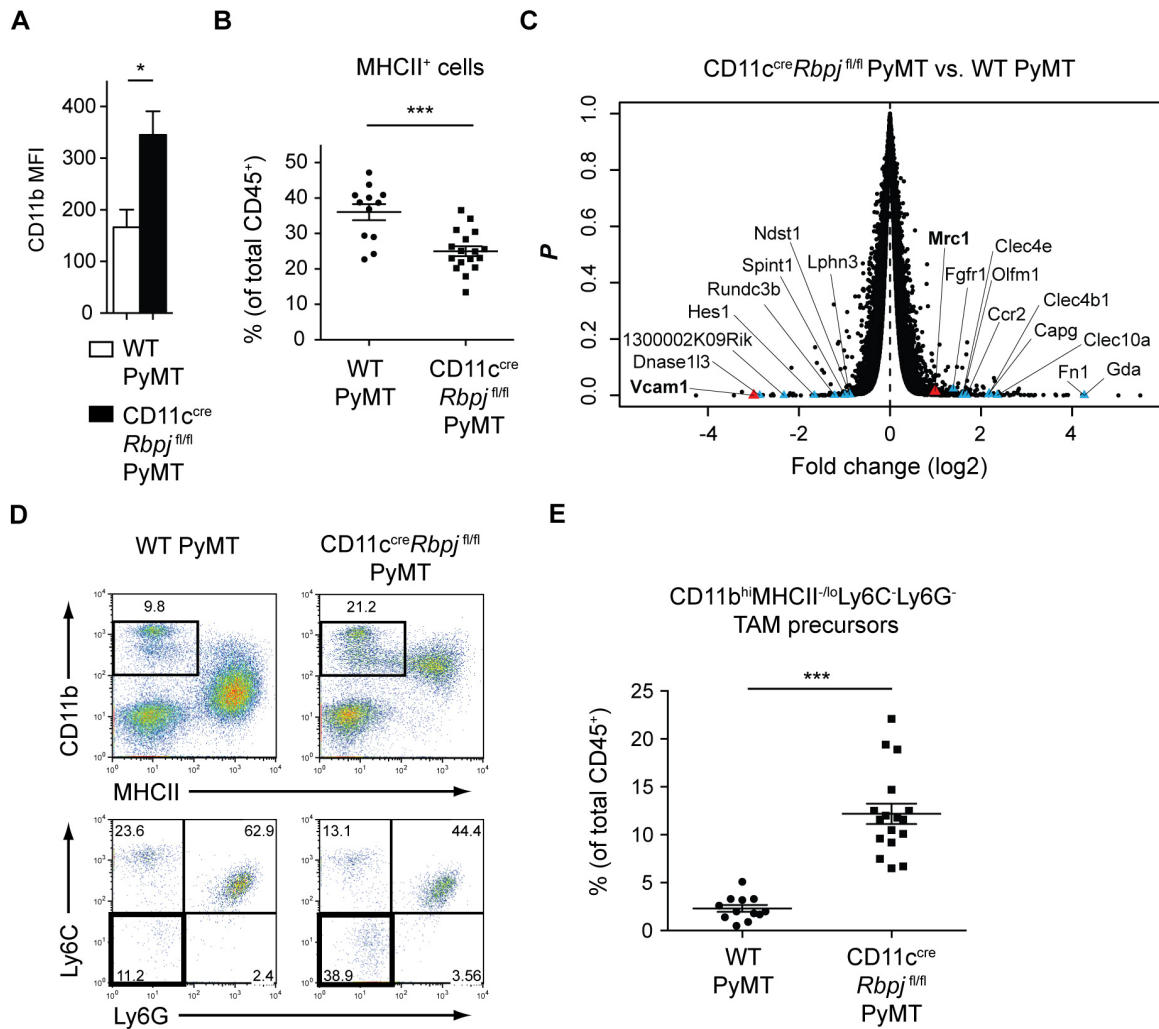


Figure S15. RBPJ is Required for TAM Terminal Differentiation

(A) Relative CD11b expression on MHCII⁺ population in 20-week-old CD11c^{cre} Rbpj^{fl/fl} PyMT and WT PyMT mice (n=4); MFI, mean fluorescence intensity. **(B)** Total CD45⁺MHCII⁺ population in CD11c^{cre} Rbpj^{fl/fl} PyMT and WT PyMT mice (n=12-17). **(C)** Volcano plot of differentially expressed genes between MHCII⁺ population in CD11c^{cre} Rbpj^{fl/fl} PyMT and MHCII⁺CD11b^{lo} population in WT PyMT mice. Blue triangles represent Notch-dependent program, red triangles: Vcam1 and Mrc1 (“P”, p value; fold change is depicted using a log scale). Expression data are pooled from 2 replicate microarray experiments. **(D)** Gating strategy for CD45⁺B220⁻CD11b^{hi}MHCII^{lo}Ly6C⁺Ly6G⁻ TAM precursors. **(E)** Quantification of data as in **(D)** (n=12-17). All comparisons were made using student’s *t* test and represent pooled data from at least 4 independent experiments. Data are shown as mean ± SEM. Statistical significance is indicated by *p < 0.05, ***p < 0.001.

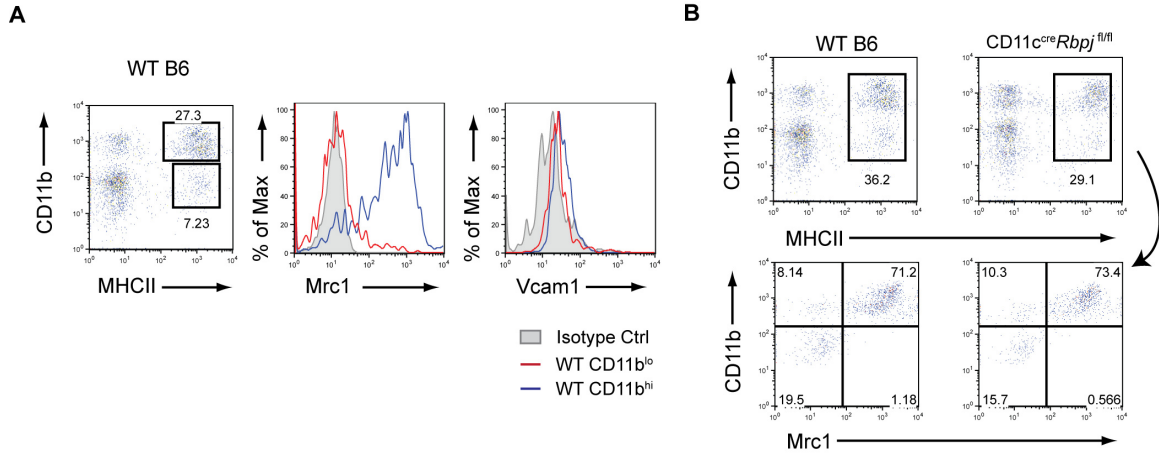


Figure S16. Myeloid Populations in Mammary Tissues from WT and CD11c^{cre} Rbpj^{fl/fl} Mice are Indistinguishable

(A) Vcam1 and Mrc1 expression on CD11b^{hi} and CD11b^o myeloid cell populations in steady state mammary glands. (B) Flow cytometric data of myeloid populations from the mammary glands of WT and CD11c^{cre} Rbpj^{fl/fl} mice. Plots are gated on CD45⁺ cells. Results are representative of 2 independent experiments.

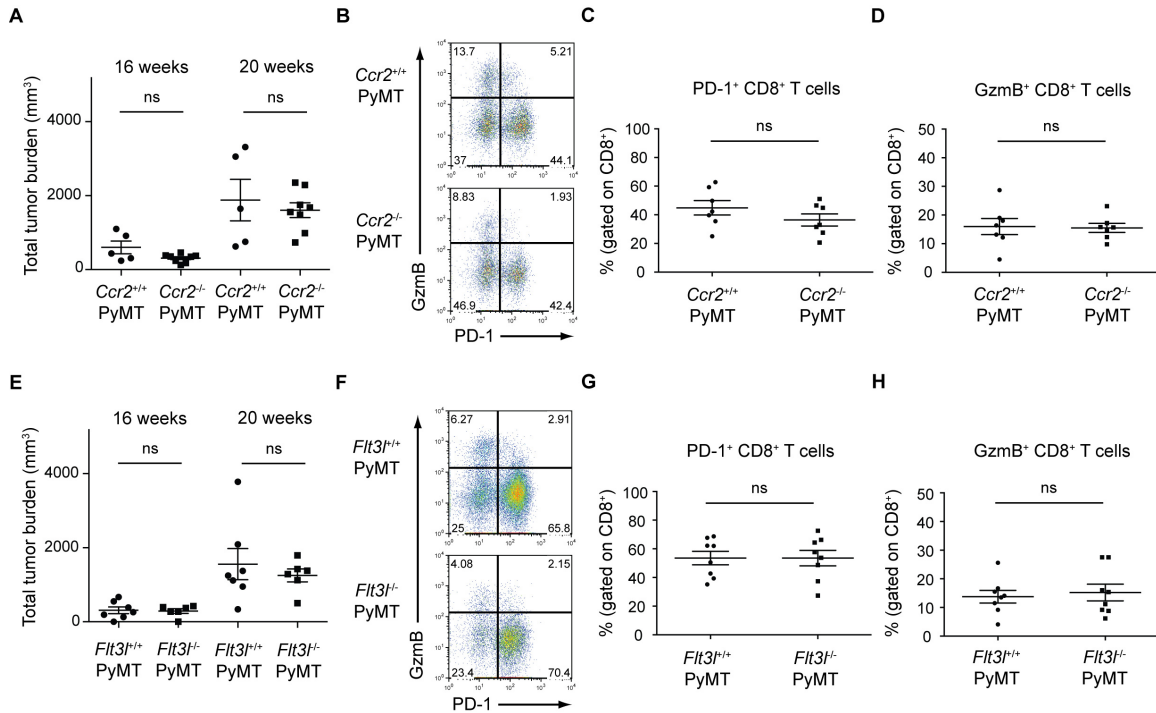


Figure S17. Loss of MTMs or Classical DCs does not Affect T Cell Phenotype or Tumor Development

(A) The total tumor burden of *Ccr2*^{+/+} PyMT and *Ccr2*^{-/-} PyMT mice at 16 and 20 weeks of age (n=5-8). **(B)** Flow cytometric analysis of PD-1 and GzmB expression in CD8⁺ T cells from *Ccr2*^{+/+} PyMT or *Ccr2*^{-/-} PyMT mice. **(C and D)** Quantification of PD-1⁺ or GzmB⁺ CD8⁺ T cells as in **(B)** (n=7). **(E)** Total tumor burden of *Flt3*^{+/+} PyMT and *Flt3*^{-/-} PyMT mice at 16 and 20 weeks of age (n=6-7). **(F)** Flow cytometric analysis of PD-1 and GzmB expression in CD8⁺ T cells from *Flt3*^{+/+} PyMT or *Flt3*^{-/-} PyMT mice. **(G and H)** Quantification of PD-1⁺ or GzmB⁺ CD8⁺ T cells as in **(F)** (n=8). All comparisons were made using student's *t* test and represent pooled data from at least 4 independent experiments. Data are shown as mean ± SEM; ns=not statistically significant.

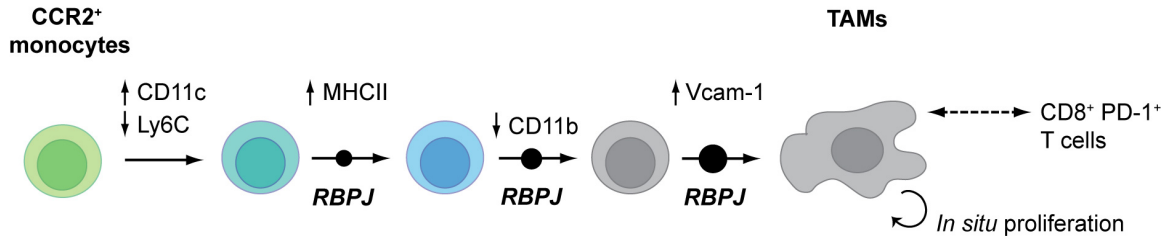


Figure S18. TAMs Differentiate from Inflammatory Monocytes

TAM differentiation occurs in phenotypically distinct steps. CD11c upregulation and Ly6C downregulation are the earliest differentiation events and occur independently of RBPJ. MHCII upregulation and CD11b downregulation occur subsequently and Vcam1 upregulation can be detected on terminally differentiated TAMs. TAMs also undergo cell proliferation within developing tumors and may affect tumor development through the modulation of CD8⁺ T cell activity.